Available online at www.sciencedirect.com

ScienceDirect

IFAC PapersOnline CONFERENCE PAPER ARCHIVE

IFAC PapersOnLine 51-29 (2018) 140–146

A Dynamic Window-Based Controller for Dynamic Positioning Satisfying Actuator Magnitude Constraints

Mikkel Eske Nørgaard Sørensen, Ole Nikolai Lyngstadaas, Bjørn-Olav H. Eriksen and Morten Breivik

Centre for Autonomous Marine Operations and Systems, Department of Engineering Cybernetics, Norwegian University of Science and Technology (NTNU), NO-7491 Trondheim, Norway
E-mail: {mikkel.e.n.sorensen, bjorn-olav.h.eriksen, morten.breivik}@ieee.org, olenl@stud.ntnu.no

Abstract: This paper considers the use of a simplified dynamic window (DW) algorithm to handle actuator magnitude constraints for a 3 degrees-of-freedom dynamic positioning controller for ships. To accomplish this, we use the simplified DW algorithm to design a dynamic window-based controller (DWC) which guarantees that the velocities remain within a feasible set, while simultaneously respecting the actuator magnitude constraints. The DWC is compared with a benchmark motion controller which uses nonlinear position and velocity feedback terms. The comparison is made using performance metrics which consider both control accuracy and energy efficiency.

Keywords: Dynamic positioning, Dynamic window, Actuator magnitude constraints

1. INTRODUCTION

Numerous ship motion controllers and autopilots have been proposed over the years. However, many control algorithms found in the literature do not explicitly consider saturation constraints for the actuators. Examples of traditional motion control designs for ships are given in (Fossen, 2011). Not considering actuator constraints may lead to unsatisfying performance or stability issues.

In (Fox et al., 1997), the dynamic window (DW) algorithm is suggested as a method to achieve collision avoidance and deal with actuator constraints imposed by limited velocities and accelerations for mobile robots. The DW algorithm is modified for AUVs in (Eriksen et al., 2016), and shows promising results for handling actuator magnitude and rate constraints. In (Sørensen et al., 2017), a simplification of this algorithm is proposed for a 2 degrees-of-freedom (DOF) heading and speed controller, by removing the collision avoidance part of the algorithm. This DW-based controller (DWC) is combined with a motion controller based on the design in (Sørensen and Breivik, 2016).

The contribution of this paper is the extension of the 2 DOF DWC presented in (Sørensen et al., 2017) to a 3 DOF DWC suitable for dynamic positioning (DP). The 3 DOF DWC is compared with a benchmark controller (BC) from (Sørensen and Breivik, 2016), where the comparison is made using performance metrics which consider both control accuracy and energy efficiency.

The rest of the paper is organized as follows: A mathematical ship model is presented in Section 2; Section 3 describes the assumptions and control objective; Section 4 presents the design of a benchmark controller inspired by backstepping and constant-bearing guidance; Section 5 presents the proposed DWC concept; Section 6 presents simulation results, while Section 7 concludes the paper.

2. SHIP MODEL

The motion of a ship can be represented by the pose vector $\boldsymbol{\eta} = [x, y, \psi]^\top \in \mathbb{R}^2 \times \mathbb{S}$ and the velocity vector $\boldsymbol{\nu} = [u, v, r]^\top \in \mathbb{R}^3$. Here, (x, y) represents the Cartesian position in a local earth-fixed reference frame, while ψ is the yaw angle. The body-fixed linear velocities are represented by (u, v), and the yaw rate is given by r. The 3 DOF dynamics of a ship can then be stated as (Fossen, 2011):

$$\dot{\boldsymbol{\eta}} = \boldsymbol{R}(\psi)\boldsymbol{\nu} \tag{1}$$

$$\boldsymbol{M}\dot{\boldsymbol{\nu}} + \boldsymbol{C}(\boldsymbol{\nu})\boldsymbol{\nu} + \boldsymbol{D}(\boldsymbol{\nu})\boldsymbol{\nu} = \boldsymbol{\tau}, \tag{2}$$

where $\boldsymbol{M} \in \mathbb{R}^{3\times3}$, $\boldsymbol{C}(\boldsymbol{\nu}) \in \mathbb{R}^{3\times3}$, $\boldsymbol{D}(\boldsymbol{\nu}) \in \mathbb{R}^{3\times3}$ and $\boldsymbol{\tau} = [\tau_1, \tau_2, \tau_3]^\top$ represent the inertia matrix, Coriolis and centripetal matrix, damping matrix and control input vector, respectively. The rotation matrix $\boldsymbol{R}(\psi) \in SO(3)$ is given as

$$\boldsymbol{R}(\psi) = \begin{bmatrix} \cos(\psi) & -\sin(\psi) & 0 \\ \sin(\psi) & \cos(\psi) & 0 \\ 0 & 0 & 1 \end{bmatrix}. \tag{3}$$

The system matrices are assumed to satisfy the properties $\boldsymbol{M} = \boldsymbol{M}^\top > 0$, $\boldsymbol{C}(\boldsymbol{\nu}) = -\boldsymbol{C}(\boldsymbol{\nu})^\top$ and $\boldsymbol{D}(\boldsymbol{\nu}) > 0$. In this paper, we use the model and parameters of the model-scale ship CyberShip Inocean CAT I Arctic Drillship (CSAD) (Bjørnø et al., 2017) for control design and evaluation through numerical simulations. CSAD is a 1:90 scale replica of the full-scale Statoil CAT I Arctic Drillship, with

2405-8963
Peer review under responsibility of International Federation of Automatic Control.
10.1016/j.ifacol.2018.09.483

a length of $L = 2.578$ m, and is shown in Fig 1. The inertia

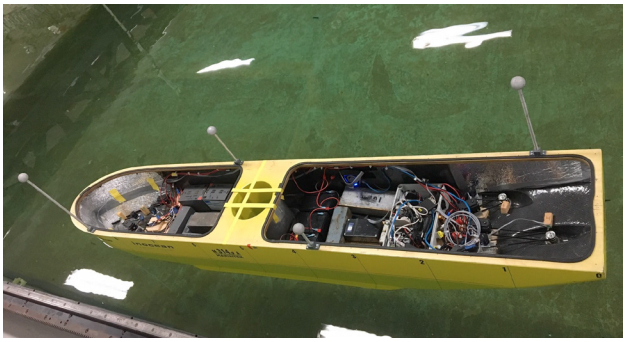

Fig. 1. CyberShip Inocean CAT I Arctic Drillship in the Marine Cybernetics Laboratory at NTNU.

matrix is given as

$$\boldsymbol{M} = \boldsymbol{M}_{RB} + \boldsymbol{M}_A, \tag{4}$$

where

$$\boldsymbol{M}_{RB} = \begin{bmatrix} m & 0 & 0 \\ 0 & m & mx_g \\ 0 & mx_g & I_z \end{bmatrix} \tag{5}$$

$$\boldsymbol{M}_A = \begin{bmatrix} -X_{\dot{u}} & 0 & 0 \\ 0 & -Y_{\dot{v}} & -Y_{\dot{r}} \\ 0 & -N_{\dot{v}} & -N_{\dot{r}} \end{bmatrix}. \tag{6}$$

The mass of CSAD is $m = 127.92$ kg, while $x_g = 0.00375$ m is the distance along the x-axis in the body frame from the center of gravity. The moment of inertia about the z-axis in the body frame is $I_z = 61.987$ kg m^2. Other parameter values are listed in Table 1. Note that N_r, which is marked in bold, has been changed to correspond better with the actual physical behavior of CSAD. The Coriolis and centripetal matrix is

$$\boldsymbol{C}(\boldsymbol{\nu}) = \boldsymbol{C}_{RB}(\boldsymbol{\nu}) + \boldsymbol{C}_A(\boldsymbol{\nu}), \tag{7}$$

with

$$\boldsymbol{C}_{RB}(\boldsymbol{\nu}) = \begin{bmatrix} 0 & 0 & -m(x_g r + v) \\ 0 & 0 & mu \\ m(x_g r + v) & -mu & 0 \end{bmatrix} \tag{8}$$

$$\boldsymbol{C}_A(\boldsymbol{\nu}) = \begin{bmatrix} 0 & 0 & -c_{A,13}(\boldsymbol{\nu}) \\ 0 & 0 & c_{A,23}(\boldsymbol{\nu}) \\ c_{A,13}(\boldsymbol{\nu}) & -c_{A,23}(\boldsymbol{\nu}) & 0 \end{bmatrix}, \tag{9}$$

where

$$c_{A,13}(\boldsymbol{\nu}) = -Y_{\dot{v}} v - \frac{1}{2}(N_{\dot{v}} + Y_{\dot{r}}) r \tag{10}$$

$$c_{A,23}(\boldsymbol{\nu}) = -X_{\dot{u}} u. \tag{11}$$

Finally, the damping matrix $\boldsymbol{D}(\boldsymbol{\nu})$ is given as

$$\boldsymbol{D}(\boldsymbol{\nu}) = \boldsymbol{D}_L + \boldsymbol{D}_{NL}(\boldsymbol{\nu}), \tag{12}$$

where

$$\boldsymbol{D}_L = \begin{bmatrix} -X_u & 0 & 0 \\ 0 & -Y_v & 0 \\ 0 & 0 & -N_r \end{bmatrix} \tag{13}$$

$$\boldsymbol{D}_{NL}(\boldsymbol{\nu}) = \begin{bmatrix} d_{NL,11}(\boldsymbol{\nu}) & 0 & 0 \\ 0 & d_{NL,22}(\boldsymbol{\nu}) & 0 \\ 0 & 0 & d_{NL,33}(\boldsymbol{\nu}) \end{bmatrix}, \tag{14}$$

and

$$d_{NL,11}(\boldsymbol{\nu}) = -X_{|u|u}|u| - X_{uuu}u^2 \tag{15}$$

$$d_{NL,22}(\boldsymbol{\nu}) = -Y_{|v|v}|v| - Y_{|r|v}|r| \tag{16}$$

$$d_{NL,33}(\boldsymbol{\nu}) = -N_{|v|r}|v| - N_{|r|r}|r|. \tag{17}$$

Table 1. Parameters for CSAD (Bjørnø et al., 2017).

Parameter	Value	Parameter	Value
$X_{\dot{u}}$	-3.262	X_{uuu}	-8.557
$Y_{\dot{v}}$	-28.89	Y_v	-4.673
$Y_{\dot{r}}$	-0.525	$Y_{\|v\|v}$	0.398
$N_{\dot{v}}$	-0.157	$Y_{\|r\|v}$	-0.805
$N_{\dot{r}}$	-13.98	$N_{\|v\|r}$	0.080
X_u	-2.332	N_r	**-6.900**
$X_{\|u\|u}$	0	$N_{\|r\|r}$	-0.0115

The considered model describes a fully actuated ship, where the actuator forces and moments are modeled using the six mounted thrusters $\boldsymbol{u} = [u_1, u_2, u_3, u_4, u_5, u_6]^\top \in \mathbb{R}^6$ (Bjørnø et al., 2017). These are related to the input vector $\boldsymbol{\tau}$ through the actuator model

$$\boldsymbol{\tau}(\boldsymbol{u}) = \boldsymbol{T}\boldsymbol{K}_T\boldsymbol{u}, \tag{18}$$

where $\boldsymbol{T} \in \mathbb{R}^{3\times 6}$ is an actuator configuration matrix, while $\boldsymbol{K}_T \in \mathbb{R}^{6\times 6}$ is an actuator force matrix. The actuator configuration matrix is

$$\boldsymbol{T} = \begin{bmatrix} c(\delta_1) & c(\delta_2) & c(\delta_3) & c(\delta_4) & c(\delta_5) & c(\delta_6) \\ s(\delta_1) & s(\delta_2) & s(\delta_3) & s(\delta_4) & s(\delta_5) & s(\delta_6) \\ \phi_1 & \phi_2 & \phi_3 & \phi_4 & \phi_5 & \phi_6 \end{bmatrix}, \tag{19}$$

where $c(\delta_i) = \cos(\delta_i)$, $s(\delta_i) = \sin(\delta_i)$. The constant $\phi_i = L_i \cos(\beta_i)\sin(\delta_i)$ with $L_i = \sqrt{L_{x,i}^2 + L_{y,i}^2}$, where $L_{x,i}$ and $L_{y,i}$ represent the physical placements of the ith actuator and $\beta_i = \text{atan}(L_{y,i}/L_{x,i})$ for $i \in [1, 6]$. The actuator force matrix is given as

$$\boldsymbol{K}_T = \text{diag}([K_{T,1}, K_{T,2}, K_{T,3}, K_{T,4}, K_{T,5}, K_{T,6}]), \tag{20}$$

where $K_{T,i} > 0$ is the thrust force from the ith propeller. In (Bjørnø et al., 2017), the actuator magnitude constraints are stated as

$$u_i \in [-0.5, 0.5]. \tag{21}$$

In this work, we fix the actuators to the following angles $\boldsymbol{\delta} = [\pi, \pi/4, -\pi/4, 0, 5\pi/4, 3\pi/4]$.

The considered ship has to move at low speeds in order to be fully actuated for DP operations. Assuming low-speed maneuvers, the kinetic model in (2) can be simplified to

$$\boldsymbol{M}\dot{\nu} + \boldsymbol{D}_L\boldsymbol{\nu} = \boldsymbol{\tau}, \tag{22}$$

since for low-speed maneuvers the linear damping will dominate over both the nonlinear damping and the Coriolis and centripetal forces (Fossen, 2011). The model (22) will be used in the control designs in the following sections.

3. ASSUMPTIONS AND CONTROL OBJECTIVE

It is assumed that both the pose vector $\boldsymbol{\eta}(t)$ and velocity vector $\boldsymbol{\nu}(t)$ can be measured, and that no disturbances and uncertainties affect the system.

The control objective is to make $\tilde{\boldsymbol{\eta}}(t) \triangleq \boldsymbol{\eta}(t) - \boldsymbol{\eta}_t(t) \to \boldsymbol{0}$ as $t \to \infty$, where $\boldsymbol{\eta}_t(t) \in \mathbb{R}^2 \times \mathbb{S}$ represents the pose associated with a virtual target ship. The motion of the target ship is typically defined by a human or generated by a guidance system.

For notational simplicity, the time t is omitted in the rest of this paper.

4. BENCHMARK CONTROLLER

In (Sørensen and Breivik, 2016), a cascaded motion controller with nonlinear pose and velocity feedback is suggested. Through its nonlinear feedback terms, this controller can partly handle actuator magnitude constraints. In this paper, this controller is modified to a low-speed DP version where the control input can be chosen as

$$\boldsymbol{\tau} = \boldsymbol{M}\dot{\boldsymbol{\alpha}} + \boldsymbol{D}_L\boldsymbol{\alpha} - \boldsymbol{K}_2(\boldsymbol{z}_2)\boldsymbol{z}_2. \tag{23}$$

The error variables $\boldsymbol{z}_1 = [z_{1,x}, z_{1,y}, z_{1,\psi}]^\top$ and $\boldsymbol{z}_2 = [z_{2,u}, z_{2,v}, z_{2,r}]^\top$ are defined as

$$\boldsymbol{z}_1 \triangleq \boldsymbol{R}^\top(\psi)(\boldsymbol{\eta} - \boldsymbol{\eta}_t) \tag{24}$$

$$\boldsymbol{z}_2 \triangleq \boldsymbol{\nu} - \boldsymbol{\alpha}, \tag{25}$$

where $\boldsymbol{\alpha} = [\alpha_u, \alpha_v, \alpha_r] \in \mathbb{R}^3$ is a vector of stabilising functions that can be interpreted as a desired velocity

$$\boldsymbol{\alpha} = \boldsymbol{R}^\top\dot{\boldsymbol{\eta}}_t - \boldsymbol{K}_1(\boldsymbol{z}_1)\boldsymbol{z}_1, \tag{26}$$

where

$$\boldsymbol{K}_1(\boldsymbol{z}_1) \triangleq \boldsymbol{\Gamma}_1 \begin{bmatrix} \frac{1}{\sqrt{\boldsymbol{z}_{1,\tilde{p}}^\top \boldsymbol{z}_{1,\tilde{p}} + \Delta_{\tilde{p}}^2}}\mathbf{I}_{2\times 2} & \mathbf{0}_{2\times 1} \\ \mathbf{0}_{1\times 2} & \frac{1}{\sqrt{z_{1,\tilde{\psi}}^2 + \Delta_{\tilde{\psi}}^2}} \end{bmatrix}, \tag{27}$$

represents a nonlinear control gain with $\boldsymbol{\Gamma}_1 > 0$, $\mathbf{z}_{1,\tilde{p}} \triangleq [z_{1,x}, z_{1,y}]^\top$, $\Delta_{\tilde{p}} > 0$ and $\Delta_{\tilde{\psi}} > 0$. The nonlinear feedback term in (23) is given as

$$\boldsymbol{K}_2(\boldsymbol{z}_2) \triangleq \boldsymbol{\Gamma}_2 \begin{bmatrix} \frac{1}{\sqrt{\boldsymbol{z}_{2,\tilde{v}}^\top \boldsymbol{z}_{2,\tilde{v}} + \Delta_{\tilde{v}}^2}}\boldsymbol{I}_{2\times 2} & \mathbf{0}_{2\times 1} \\ \mathbf{0}_{1\times 2} & \frac{1}{\sqrt{z_{2,\tilde{r}}^2 + \Delta_{\tilde{r}}^2}} \end{bmatrix}, \tag{28}$$

with the control gain $\boldsymbol{\Gamma}_2 > 0$, where $\boldsymbol{z}_{2,\tilde{v}} \triangleq [z_{2,u}, z_{2,v}]^\top$, $\Delta_{\tilde{v}} > 0$ and $\Delta_{\tilde{r}} > 0$. The time derivative of $\boldsymbol{\alpha}$ is

$$\dot{\boldsymbol{\alpha}} = \boldsymbol{R}^\top\ddot{\boldsymbol{\eta}}_t + \boldsymbol{S}^\top\boldsymbol{R}^\top\dot{\boldsymbol{\eta}}_t - \dot{\boldsymbol{K}}_1(\boldsymbol{z}_1)\boldsymbol{z}_1 - \boldsymbol{K}_1(\boldsymbol{z}_1)\dot{\boldsymbol{z}}_1, \tag{29}$$

where

$$\dot{\boldsymbol{K}}_1(\boldsymbol{z}_1) = -\boldsymbol{\Gamma}_1 \begin{bmatrix} \frac{\boldsymbol{z}_{1,\tilde{p}}^\top \dot{\boldsymbol{z}}_{1,\tilde{p}}}{(\boldsymbol{z}_{1,\tilde{p}}^\top \boldsymbol{z}_{1,\tilde{p}} + \Delta_{\tilde{p}}^2)^{\frac{3}{2}}}\boldsymbol{I}_{2\times 2} & \mathbf{0}_{2\times 1} \\ \mathbf{0}_{1\times 2} & \frac{z_{1,\tilde{\psi}}\dot{z}_{1,\tilde{\psi}}}{(z_{1,\tilde{\psi}}^2 + \Delta_{\tilde{\psi}}^2)^{\frac{3}{2}}} \end{bmatrix}, \tag{30}$$

with

$$\dot{\boldsymbol{z}}_1 = \boldsymbol{S}^\top\boldsymbol{z}_1 - \boldsymbol{K}_1(\boldsymbol{z}_1)\boldsymbol{z}_1 + \boldsymbol{z}_2, \tag{31}$$

where

$$\mathbf{S}(r) = \begin{bmatrix} 0 & -r & 0 \\ r & 0 & 0 \\ 0 & 0 & 0 \end{bmatrix} \tag{32}$$

is a skew-symmetric matrix satisfying $\mathbf{z}_1^\top\mathbf{S}(r)^\top\mathbf{z}_1 = 0$.

5. DYNAMIC WINDOW-BASED CONTROL DESIGN

5.1 Simplified Dynamic Window Algorithm

Here, we present a 3 DOF extension to the 2 DOF DWC controller suggested in (Sørensen et al., 2017).

Based on the ship model and its actuator magnitude constraints, a set of possible velocities can be found. This set contains all the velocities the ship can achieve with respect to the actuator magnitude constraints. The possible velocities can be found by computing the steady-state solutions of the kinetics of (22) for all possible control inputs:

$$\boldsymbol{\tau}(\boldsymbol{u}) = \boldsymbol{D}_L\boldsymbol{\nu}_{ss}, \tag{33}$$

within the actuator magnitude constraints shown in (21). The steady-state solutions of (33) for a uniformly distributed set of control inputs are shown in Fig. 2. The

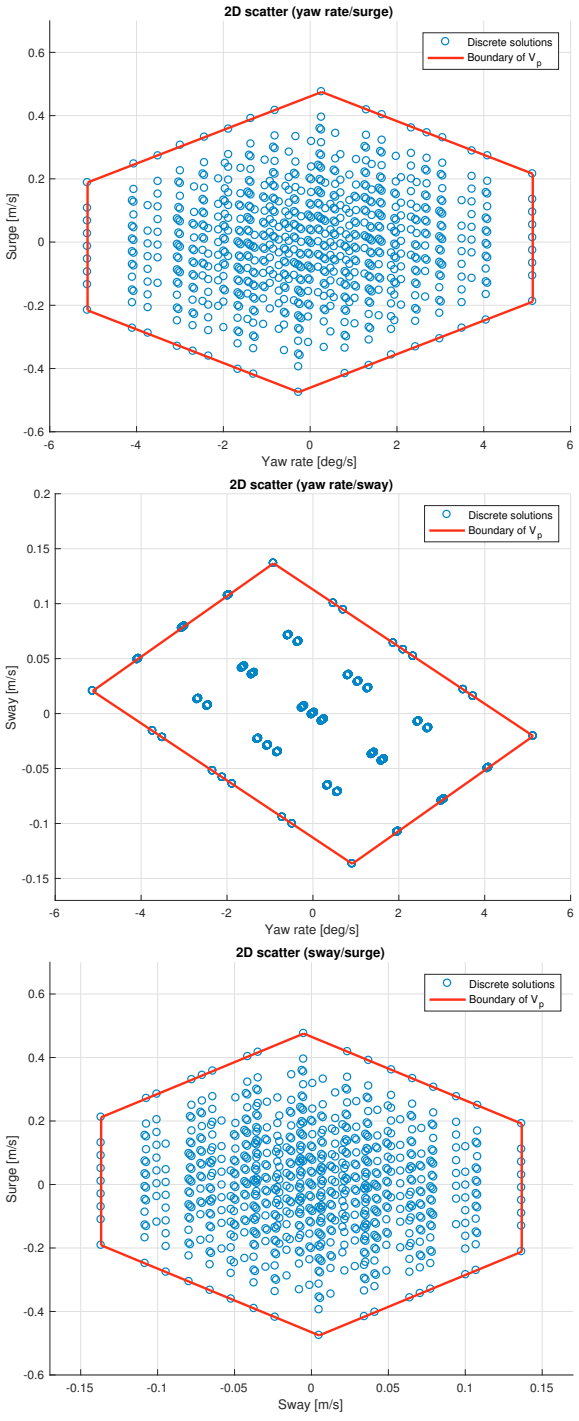

Fig. 2. Possible combinations of surge speed, sway speed and yaw rate, with respect to the actuator magnitude saturation limits.

set of possible velocities can be defined as

$$V_p = \{(u, v, r) \in \mathbb{R} \times \mathbb{R} \times \mathbb{R} \mid g(u, v, r) \geq 0\}, \tag{34}$$

where $g(u, v, r)$ is a positive semidefinite function for feasible velocities with respect to the actuator constraints. An approximation of the 3 DOF set is done by projecting the set into three 2 DOF sets to simplify calculations. We justify this approximation by noting that each of the

steady-state solution boundary faces are almost parallel with one axis, see Fig. 2. Following this, faces that are parallel with one axis can be parameterized by the remaining two variables. Notice, however, that we lose information where all three variables are correlated, and can therefore not model faces which are not parallel with one of the axes. The result of the approximation is the following three sets of possible velocities:

$$V_{p,(u,r)} = \{(u,r) \in \mathbb{R} \times \mathbb{R} \mid g_{(u,r)}(u,r) \geq 0\} \quad (35)$$

$$V_{p,(v,r)} = \{(v,r) \in \mathbb{R} \times \mathbb{R} \mid g_{(v,r)}(v,r) \geq 0\} \quad (36)$$

$$V_{p,(u,v)} = \{(u,v) \in \mathbb{R} \times \mathbb{R} \mid g_{(u,v)}(u,v) \geq 0\}, \quad (37)$$

where $g_{(u,r)}(u,r)$, $g_{(v,r)}(v,r)$ and $g_{(u,v)}(u,v)$ are greater than or equal to zero for velocities inside the corresponding boundaries. Given m, n and k approximated boundaries, defined by the functions $h_{a,(u,r)}(u,r) = h_{b,(v,r)}(v,r) = h_{c,(u,v)}(u,v) = 0$, $a \in \{1,2,...,m\}$, $b \in \{1,2,...,n\}$ and $c \in \{1,2,...,k\}$, the approximated functions are given as:

$$g_{(u,r)}(u,r) = \min(h_{1,(u,r)}(u,r), h_{2,(u,r)}(u,r), ..., h_{m,(u,r)}(u,r)) \quad (38)$$

$$g_{(v,r)}(v,r) = \min(h_{1,(v,r)}(v,r), h_{2,(v,r)}(v,r), ..., h_{n,(v,r)}(v,r)) \quad (39)$$

$$g_{(u,v)}(u,v) = \min(h_{1,(u,v)}(u,v), h_{2,(u,v)}(u,v), , ..., h_{k,(u,v)}(u,v)). \quad (40)$$

Here, the functions $h_{a,(u,r)}(u,r) = h_{b,(v,r)}(v,r) = h_{c,(u,v)}(u,v) = 0$ are defined by using regression on the boundary of the sets $V_{p_{(u,r)}}$, $V_{p_{(v,r)}}$ and $V_{p_{(u,v)}}$, where $\nabla h_{a,(u,r)}(u,r)$, $\nabla h_{b,(v,r)}(v,r)$ and $\nabla h_{c,(u,v)}(u,v)$ are required to be pointing inwards to the valid solutions.

Next, the space of reachable points within one time step T needs to be defined. Using

$$\dot{\boldsymbol{\nu}}_{min} = [\dot{u}_{min}, \dot{v}_{min}, \dot{r}_{min}] = \boldsymbol{M}^{-1}(\boldsymbol{\tau}_{min}(\boldsymbol{u}) - \boldsymbol{D}_L \boldsymbol{\nu}^*) \quad (41)$$

$$\dot{\boldsymbol{\nu}}_{max} = [\dot{u}_{max}, \dot{v}_{max}, \dot{r}_{max}] = \boldsymbol{M}^{-1}(\boldsymbol{\tau}_{max}(\boldsymbol{u}) - \boldsymbol{D}_L \boldsymbol{\nu}^*), \quad (42)$$

where $\boldsymbol{\nu}^*$ is the current velocity of $\boldsymbol{\nu}(t)$, we find the acceleration limits and the reachable velocities for the current time step, resulting in the dynamic velocity window

$$\begin{aligned} V_w = \{(u,v,r) \in \mathbb{R} \times \mathbb{R} \times \mathbb{R} \mid \\ u \in [u^* + \dot{u}_{min}T, u^* + \dot{u}_{max}T] \\ \wedge\, v \in [v^* + \dot{v}_{min}T, v^* + \dot{v}_{max}T] \\ \wedge\, r \in [r^* + \dot{r}_{min}T, r^* + \dot{r}_{max}T]\}, \end{aligned} \quad (43)$$

which we project into the three cases

$$\begin{aligned} V_{w,(u,r)} = \{(u,r) \in \mathbb{R} \times \mathbb{R} \mid u \in [u^* + \dot{u}_{min}T, u^* + \dot{u}_{max}T] \\ \wedge\, r \in [r^* + \dot{r}_{min}T, r^* + \dot{r}_{max}T]\} \end{aligned} \quad (44)$$

$$\begin{aligned} V_{w,(v,r)} = \{(v,r) \in \mathbb{R} \times \mathbb{R} \mid v \in [v^* + \dot{v}_{min}T, v^* + \dot{v}_{max}T] \\ \wedge\, r \in [r^* + \dot{r}_{min}T, r^* + \dot{r}_{max}T]\} \end{aligned} \quad (45)$$

$$\begin{aligned} V_{w,(u,v)} = \{(u,v) \in \mathbb{R} \times \mathbb{R} \mid u \in [u^* + \dot{u}_{min}T, u^* + \dot{u}_{max}T] \\ \wedge\, v \in [v^* + \dot{v}_{min}T, v^* + \dot{v}_{max}T]\}. \end{aligned} \quad (46)$$

This defines the sets of dynamically feasible velocities as

$$V_{f,(u,r)} \triangleq V_{p,(u,r)} \cap V_{w,(u,r)} \quad (47)$$

$$V_{f,(v,r)} \triangleq V_{p,(v,r)} \cap V_{w,(v,r)} \quad (48)$$

$$V_{f,(u,v)} \triangleq V_{p,(u,v)} \cap V_{w,(u,v)}. \quad (49)$$

Next, the sets of dynamically feasible velocities are discretised uniformly to obtain discrete sets of dynamically feasible velocities.

For the 3 DOF case, the desired velocity is defined as

$$\boldsymbol{\nu}_d \triangleq [u_d, v_d, r_d]^\top. \quad (50)$$

Given $\boldsymbol{\nu}_d$, the optimal dynamically feasible velocity $\boldsymbol{\nu}_f \triangleq [u_f, v_f, r_f]^\top$ can be selected as

$$\boldsymbol{\nu}_f = \underset{(u,v,r) \in V_f}{\operatorname{argmax}} G(\boldsymbol{\nu}, \boldsymbol{\nu}_d), \quad (51)$$

where V_f is the general 3 DOF set and $G(\boldsymbol{\nu}, \boldsymbol{\nu}_d)$ is an objective function which is defined as

$$\begin{aligned} G(\boldsymbol{\nu}, \boldsymbol{\nu}_d) \triangleq \text{surge}(u, u_d) + \text{sway}(v, v_d) \\ + \text{yawrate}(r, r_d), \end{aligned} \quad (52)$$

with

$$\text{surge}(u, u_d) = 1 - \frac{|u_d - u|}{\max_{u' \in V_f}(|u_d - u'|)} \in [0,1] \quad (53)$$

$$\text{sway}(v, v_d) = 1 - \frac{|v_d - v|}{\max_{v' \in V_f}(|v_d - v'|)} \in [0,1] \quad (54)$$

$$\text{yawrate}(r, r_d) = 1 - \frac{|r_d - r|}{\max_{r' \in V_f}(|r_d - r'|)} \in [0,1]. \quad (55)$$

Notice that by using this objective function, we minimise the scaled 1-norm of the entire discrete set of dynamically feasible velocity.

For the three 2 DOF cases, this algorithm is modified to fit 2 DOF and run once for each velocity pair scenario; surge speed and yaw rate, sway speed and yaw rate, and surge and sway speed. Hence, it results in the three components of dynamically feasible velocities

$$\boldsymbol{\nu}_{f,(u,r)} = [\nu_{f,u}, 0, \nu_{f,r}]^\top \quad (56)$$

$$\boldsymbol{\nu}_{f,(v,r)} = [0, \nu_{f,v}, \nu_{f,r}]^\top \quad (57)$$

$$\boldsymbol{\nu}_{f,(u,v)} = [\nu_{f,u}, \nu_{f,v}, 0]^\top, \quad (58)$$

which combines into

$$\boldsymbol{\nu}_f = \frac{\boldsymbol{\nu}_{f,(u,r)} + \boldsymbol{\nu}_{f,(v,r)} + \boldsymbol{\nu}_{f,(u,v)}}{2} \quad (59)$$

for the full 3 DOF case. Fig. 3 illustrates V_p, V_w, V_f and $\boldsymbol{\nu}_d = [0.15 \text{ m/s}, -0.07 \text{ m/s}, -1.4324 \text{ deg/s}]$ given a current velocity $\boldsymbol{\nu}^* = [0.2 \text{ m/s}, -0.05 \text{ m/s} -1.1459 \text{ deg/s}]$.

5.2 Dynamic Window-based Controller

We now combine elements from the benchmark controller with the simplified DW algorithm in order to develop a dynamic window-based controller (DWC). In this setup, the simplified DW algorithm will use $\boldsymbol{\alpha} = [\alpha_u, \alpha_v, \alpha_r]^\top$ as an input such that $\boldsymbol{\nu}_d = \boldsymbol{\alpha}$. In the case where $\boldsymbol{\alpha}$ is an infeasible velocity, the simplified DW algorithm will modify $\boldsymbol{\alpha}$ to a feasible velocity $\boldsymbol{\alpha}_f = [\alpha_{f,u}, \alpha_{f,v}, \alpha_{f,r}]^\top$, otherwise $\boldsymbol{\alpha}_f = \boldsymbol{\alpha}$. Per definition, the ship will be able to achieve $\boldsymbol{\alpha}_f$ after time step T, hence the desired acceleration is chosen to be

$$\dot{\boldsymbol{\alpha}}_{DWC} = \frac{\boldsymbol{\alpha}_f - \boldsymbol{\nu}}{T}, \quad (60)$$

and

$$\boldsymbol{\alpha}_{DWC} = \int_0^t \dot{\boldsymbol{\alpha}}_{DWC}(\sigma) d\sigma + \boldsymbol{\alpha}_{DWC}(0). \quad (61)$$

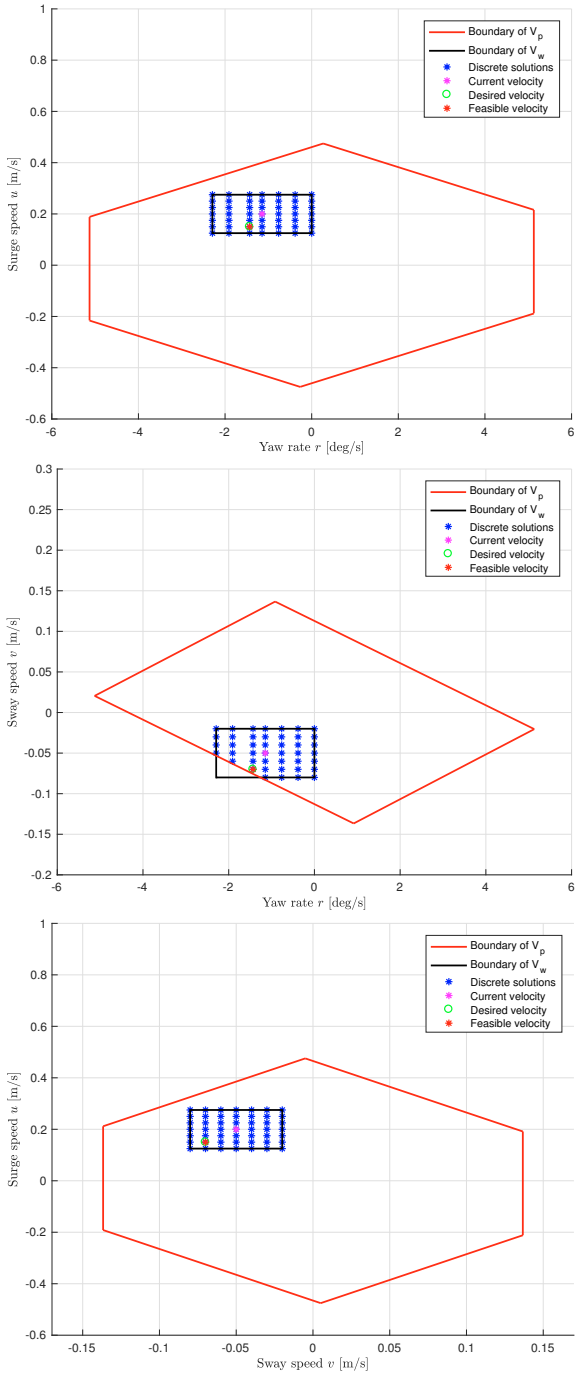

Fig. 3. The dynamically feasible velocity sets, surrounded by the boundaries of the dynamic velocity window and the set of possible velocities.

Both $\boldsymbol{\alpha}_{DWC}$ and $\dot{\boldsymbol{\alpha}}_{DWC}$ are used in the kinetic controller (23) which is modified to

$$\boldsymbol{\tau} = \boldsymbol{M}\dot{\boldsymbol{\alpha}}_{DWC} + \boldsymbol{D}_L\boldsymbol{\alpha}_{DWC}. \tag{62}$$

When comparing the control law (62) against (23), it can be seen that the explicit feedback term $-\boldsymbol{K}_2(\boldsymbol{z}_2)\boldsymbol{z}_2$ in (23) is not included in (62) since the DWC makes the feasible velocity track the derired velocity by using (60)-(61). Hence, (62) shows that the DWC is a feedforward-based control algorithm with implicity velocity feedback through α_{DWC}. However, augmenting the controller with explicit feedback terms and adaptive terms to robustify it against modeling uncertainties and unknown disturbances will not be done in this paper, but is considered future work.

6. SIMULATION RESULTS

In this section, we present numerical simulation results comparing the performance of the DWC against the benchmark controller using the full nonlinear ship model and actuator constraints of CSAD presented in Section 2. In particular, the performance is evaluated using two specific performance metrics which consider both control accuracy and energy efficiency.

The target to be tracked is defined as a changing setpoint in a 4-corner test(Skjetne et al., 2017). This test first tests the surge, sway and yaw motion individually and then increase the complexity of the task until the ship needs to do a combined surge, sway and yaw motion. In this test we use set-point tracking. Since the 4-corner test involves setpoint tracking, $\dot{\boldsymbol{\eta}}_t = \boldsymbol{0}$ and $\ddot{\boldsymbol{\eta}}_t = \boldsymbol{0}$ in (26) and (29). The initial ship states are chosen to be $\boldsymbol{\eta}(0) = [5, 1, 0]$ and $\boldsymbol{\nu}(0) = \boldsymbol{0}$. The control gains are listed in Table 2, which are chosen such that the benchmark controller (BC) does not exceed the magnitude saturation constraints and follow the tuning rules suggested in (Sørensen et al., 2018).

Table 2. Control gains.

	BC	**DWC**
$\boldsymbol{\Gamma}_1$	$\text{diag}([0.03, 0.03, 0.0349])$	$-\|\|-$
$\boldsymbol{\Gamma}_2$	$\text{diag}([0.2, 0.12, 0.1745])\boldsymbol{M}$	N/A
$\Delta_{\tilde{p},\tilde{\psi}}$	$[0.5, 0.5]$	$-\|\|-$
$\Delta_{\tilde{v},\tilde{r}}$	$[0.7, 1]$	N/A

6.1 Performance Metrics

To evaluate and compare the performance of the controllers, two performance metrics are used. We define

$$e(t) \triangleq \sqrt{\bar{\boldsymbol{\eta}}(t)^\top \bar{\boldsymbol{\eta}}(t)}, \tag{63}$$

as the error input for the performance metrics, with $\bar{\boldsymbol{\eta}}$ being the normalized signal of $\tilde{\boldsymbol{\eta}} = [\tilde{x}, \tilde{y}, \tilde{\psi}]^\top \triangleq \boldsymbol{\eta} - \boldsymbol{\eta}_t$, where $\bar{x}$, $\bar{y}$ and $\bar{\psi}$ are in the intervals $[-0.5, 0.5]$ in the expected operational space of the ship (Eriksen and Breivik, 2017). These signals represent the instantaneous control errors, while we would like to consider the accumulated errors over time. Therefore, we use the performance metric integral of the absolute error (IAE)

$$IAE(t) \triangleq \int_0^t |e(\sigma)| d\sigma, \tag{64}$$

which integrates the temporal evolution of the absolute error. We also consider the integral of the absolute error multiplied by the energy consumption (IAEW) as (Sørensen and Breivik, 2015)

$$IAEW(t) \triangleq \int_0^t |e(\sigma)| d\sigma \int_0^t P(\sigma) d\sigma, \tag{65}$$

where

$$P(t) = |\boldsymbol{\nu}(t)^\top \boldsymbol{\tau}(t)| \tag{66}$$

represents the mechanical power. IAEW thus indicates which controller has the best combined control accuracy and energy use in one single metric.

6.2 Simulation Results

In Fig. 4, the outline of the ship pose is plotted to show the transient motion behavior associated with performing the 4-corner test using the two controllers.

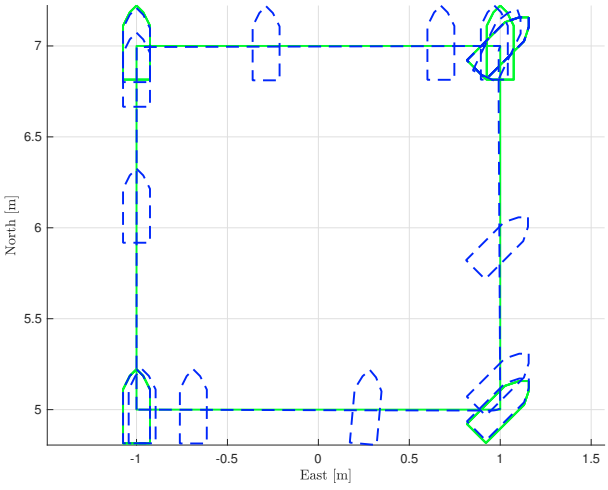

Using DWC.

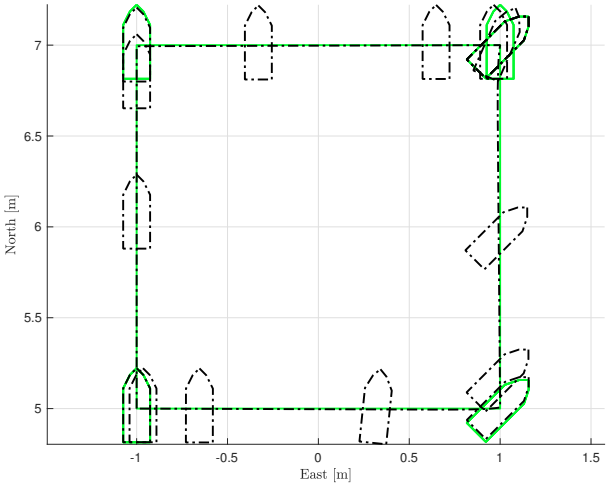

Using BC.

Fig. 4. The 4-corner test, where the dashed blue outline represents the DWC-controlled ship, the dash-dotted black outline represents the BC-controlled ship, while the green outline represents the setpoints of the 4-corner box.

Fig. 5 shows the pose of the ship together with the target pose. It can be seen that both control laws are able to track the target pose setpoints even though the DWC does not have a traditional velocity feedback term as in (23). Additionally, iit can be seen that the DWC is slightly faster than the BC controller to track the target pose setpoints.

Fig. 6 shows that the DWC commands the control inputs to stay just below the maximum magnitude constraints of the actuators, while BC is tuned such that it does not exceed the magnitude constraints. The DWC keeps the control inputs high longer than the BC, since the DWC tracks the feasible velocity $\boldsymbol{\alpha}_f$ which is on the boundaries of the windows unless the desired velocity $\boldsymbol{\alpha}$ is inside the velocity window, while the control inputs from BC have a more conservative behavior.

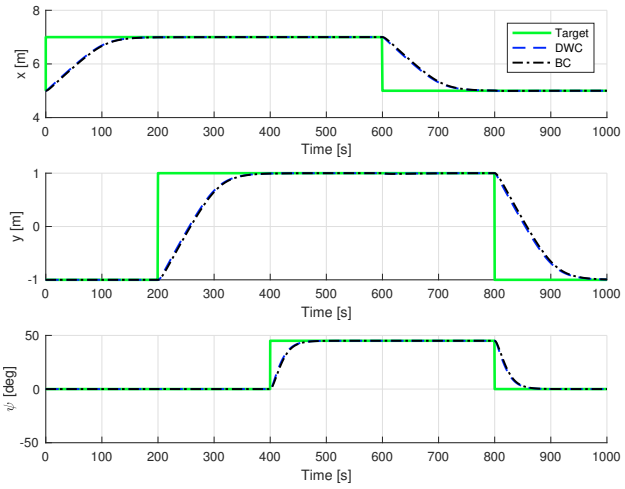

Fig. 5. Tracking the target pose.

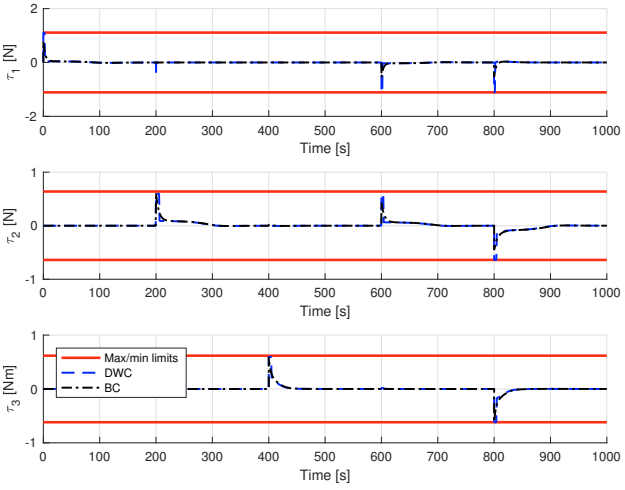

Fig. 6. The commanded control inputs with magnitude saturation limits.

Fig. 7 illustrates how the surge speed, sway speed and yaw rate moves in the velocity space in order to track α through the 4-corner test. The velocities of the ship are small in magnitude while performing the 4-corner test, constituting low-speed DP maneuvers satisfying the assumptions for using a linear ship model.

In Fig. 8, the performance metrics IAE and IAEW are shown. In particular, the IAE trajectory in the left of Fig. 8 confirms that the DWC has a slightly faster transient response since it converges faster to a stationary value. The IAEW trajectory in the right of Fig. 8 shows that the DWC has a slightly better overall performance than the benchmark controller when taking both control accuracy and energy use into account.

7. CONCLUSION

This paper has proposed an extension of a simplified dynamic window algorithm from 2 DOF to 3 DOF, as a way to ensure that the actuator magnitude constraints of a fully actuated ship are satisfied. This algorithm has been used in a dynamic window-based controller (DWC) to guarantee that ship velocities remain within a feasible set. TThe controllers are compared through numerical

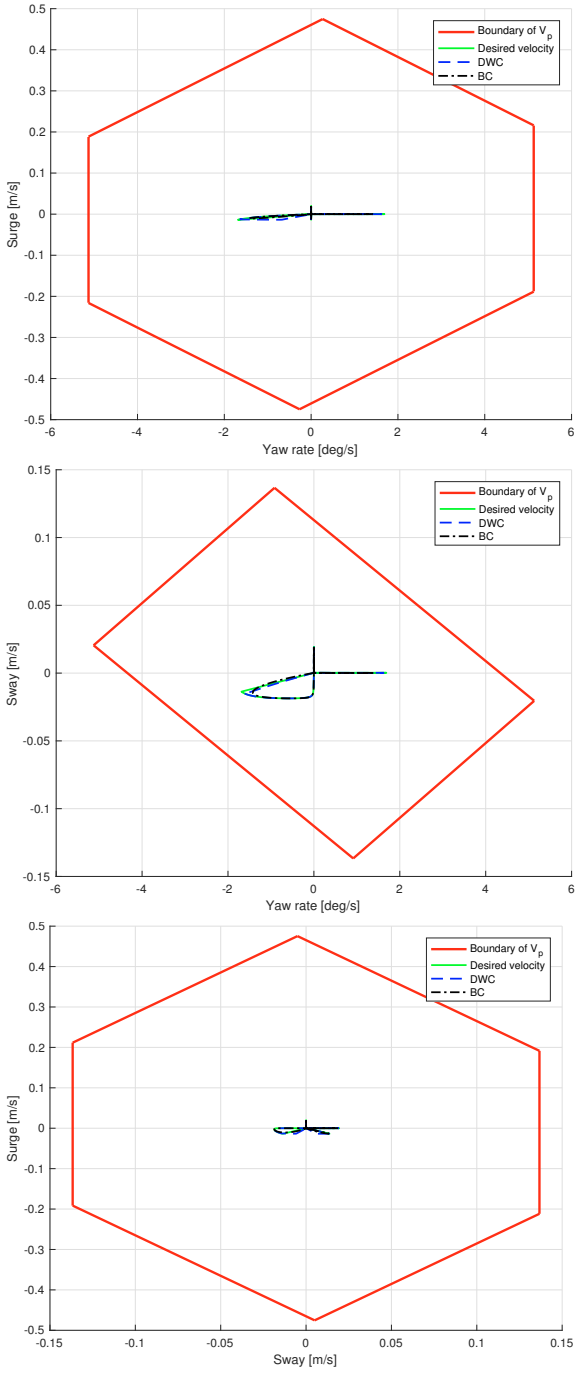

Fig. 7. Velocity trajectories in the set of possible velocities V_p.

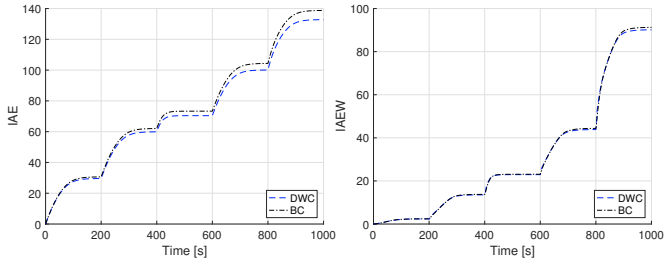

Fig. 8. IAE and IAEW performance metrics.

simulations with a fully actuated drillship performing a low-speed 4-corner dynamic positioning test, using two performance metrics to quantify the motion control behavior. The simulation results show that the proposed 3-DOF DWC controller has good tracking performance and is able to handle actuator magnitude constraints.

Future work includes exploring the robustness of the DWC controller to modeling uncertainties and unknown disturbances affecting the system. It is also relevant to consider the stability properties of the DWC controller. In addition, it is desirable to consider actuator rate constraints in addition to magnitude constraints. Finally, it is desirable to experimentally verify the results by testing the methods on a model-scale ship in an ocean basin.

ACKNOWLEDGEMENTS

This work was supported by the Research Council of Norway through the Centres of Excellence funding scheme, project number 223254.

REFERENCES

Bjørnø, J., Heyn, H.M., Skjetne, R., Dahl, A.R., and Frederich, P. (2017). Modeling, parameter identification and thruster-assisted position mooring of C/S Inocean CAT I Drillship. *in Proceedings of the 36th International Conference on Ocean, Offshore and Arctic Engineering, Trondheim, Norway.*

Eriksen, B.-O. H., Breivik, M., Pettersen, K.Y., and Wiig, M.S. (2016). A modified dynamic window algorithm for horizontal collision avoidance for AUVs. *in Proceedings of the IEEE Multi-Conference on Systems and Control, Buenos Aires, Argentina.*

Eriksen, B.-O. H. and Breivik, M. (2017). *Modeling, Identification and Control of High-Speed ASVs: Theory and Experiments*, 407–431. Sensing and Control for Autonomous Vehicles: Applications to Land, Water and Air Vehicles, Springer International Publishing.

Fossen, T.I. (2011). *Handbook of Marine Craft Hydrodynamics and Motion Control.* Wiley.

Fox, D., Burgard, W., and Thrun, S. (1997). The dynamic window approach to collision avoidance. *IEEE Robotics & Automation Magazine*, 4(1), 23–33.

Skjetne, R., Sørensen, M.E.N., Breivik, M., Værnø, S.A.T., Brodtkorb, A.H., Sørensen, A.J., Kjerstad, Ø.K., Calabrò, V., and Vinje, B.O. (2017). AMOS DP research cruise 2016: Academic full-scale testing of experimental dynamic positioning control algorithms onboard R/V Gunnerus. *in Proceedings of the 36th International Conference on Ocean, Offshore and Arctic Engineering, Trondheim, Norway.*

Sørensen, M.E.N. and Breivik, M. (2015). Comparing nonlinear adaptive motion controllers for marine surface vessels. *in Proceedings of the 10th IFAC Conference on Manoeuvring and Control of Marine Craft, Copenhagen, Denmark.*

Sørensen, M.E.N. and Breivik, M. (2016). Comparing combinations of linear and nonlinear feedback terms for motion control of marine surface vessels. *in Proceedings of the 10th IFAC Conference on Control Applications in Marine Systems, Trondheim, Norway.*

Sørensen, M.E.N., Breivik, M., and Skjetne, R. (2018). Comparing combinations of linear and nonlinear feedback terms for motion control of marine surface vessels. *submitted to IEEE Transactions on Control Systems Technology.*

Sørensen, M.E.N., Eriksen, B.-O. H., and Breivik, M. (2017). A ship heading and speed control concept inherently satisfying actuator constraints. *in Proceedings of the 1st IEEE Conference on Control Technology and Applications, Hawai'i, USA.*